THE ASTROPHYSICAL JOURNAL, 470:L15–L18, 1996 October 10

ROSAT HRI OBSERVATIONS OF CENTAURUS A

S. DÖBEREINER
Max-Planck-Institut für Extraterrestrische Physik, Karl-Schwarzschild-Strasse 1, D-85740 Garching, Germany
N. JUNKES
Astronomisches Institut Potsdam, An der Sternwarte 16, D-14482 Potsdam, Germany
S. J. WAGNER
Landessternwarte Heidelberg, Königsstuhl, D-69117 Heidelberg, Germany
H. ZINNECKER
Astronomisches Institut Potsdam, An der Sternwarte 16, D-14482 Potsdam, Germany
R. FOSBURY
Space Telescope European Coordinating Facility, European Southern Observatory, Karl-Schwarzschild-Strasse 2, D-85748 Garching, Germany
G. FABBIANO
Harvard-Smithsonian Center for Astrophysics, 60 Garden Street, Cambridge, MA 02138
AND
E. J. SCHREIER
Space Telescope Science Institute, 3700 San Martin Drive, Baltimore, MD 21218
Received 1996 April 1; accepted 1996 July 30

ABSTRACT

We present results from a sensitive high-resolution X-ray observation of the nearby active galaxy Centaurus A (NGC 5128) with the *ROSAT* high-resolution imager (HRI). The 65 ks X-ray image clearly distinguishes different components of the X-ray emission from Cen A: the nucleus and the jet, the diffuse galaxy halo, and a number of individual sources associated with the galaxy. The luminosity of the nucleus increased by a factor of 2 compared to an earlier *ROSAT* observation in 1990. The high spatial resolution of the *ROSAT* HRI shows that most of the knots in the jet are extended both along and perpendicular to the jet axis. We report the detection of a new X-ray feature, at the opposite side of the X-ray jet, which is probably due to compression of hot interstellar gas by the expanding southwestern inner radio lobe.

Subject headings: galaxies: active — galaxies: individual (Centaurus A) — galaxies: jets — X-rays: galaxies

1. INTRODUCTION

The nearby active galaxy Centaurus A (Cen A or NGC 5128) is one of the most interesting objects in the sky. With a distance of 3.5 Mpc (Hui et al. 1993), it is the closest active galaxy to the Milky Way and thus allows us to study different constituents in great detail. The optical morphology is characterized by a more or less normal stellar spheroid, bisected by a dense ring or disk of dust and gas interpreted as the remains of a recent merger with a smaller dust-rich spiral (e.g., Thomson 1992), which may also induce the nuclear activity. Radio observations reveal an active nucleus and two sets of radio lobes, the outer pair of lobes extending to 9° (several 100 kpc), the inner pair extending to 6′ on the sky. The radio structure of Cen A has been investigated in different spatial scales, including the large-scale outer lobes (Junkes et al. 1993), the inner lobes and the jet of the galaxy (Burns, Feigelson, & Schreier 1983; Clarke, Burns, & Norman 1992), and details of the central part at parsec scale (Tingay 1994). X-ray observations with the *Einstein Observatory* showed a pronounced one-sided X-ray jet, consisting of several knots and extending ≈4′ to the northeast, making it the best-observable X-ray jet (Feigelson et al. 1981). With the new sensitive *ROSAT* high-resolution imager (HRI) observations, we are able to examine the X-ray jet and other X-ray–emitting components of Cen A in much more detail.

2. OBSERVATIONS

Cen A was observed by *ROSAT* on three occasions. During the initial calibration phase of *ROSAT*, Cen A was one of the calibration targets for *ROSAT*. It was observed for 14,159 s with the *ROSAT* position-sensitive proportional counter (PSPC) and again for 19,650 s with the higher resolution HRI in 1990 July. The quality of these early *ROSAT* observations was already better than previous observations with the *Einstein Observatory*. In 1994 August Cen A was reobserved with the *ROSAT* HRI with an exposure time of 64,751 s.

The *ROSAT* HRI has a usable field of view of $40' \times 40'$. Over the total field of view, the spatial resolution is of the order of 6″ FWHM. The sensitivity is about 4 times higher than with the *Einstein* HRI. The usable energy range is 0.1–2.4 keV. The spectral resolution of the *ROSAT* HRI is nearly nonexistent, with $\Delta E/E = 0.7$, but is sufficient to differentiate between hard and soft sources on a relative basis.

3. COMPONENTS OF THE X-RAY EMISSION OF CEN A

The new X-ray data allow us to analyze structures in the central region of Cen A and to compare the X-ray features to radio and optical features, including nucleus, jet, inner radio lobes, the stellar spheroid, and the absorbing dust lane.

Figure 1 (Plate L2) shows an enlargement of the HRI X-ray image. For this image the data of the HRI observations in 1990 and 1994 have been combined. The field size is

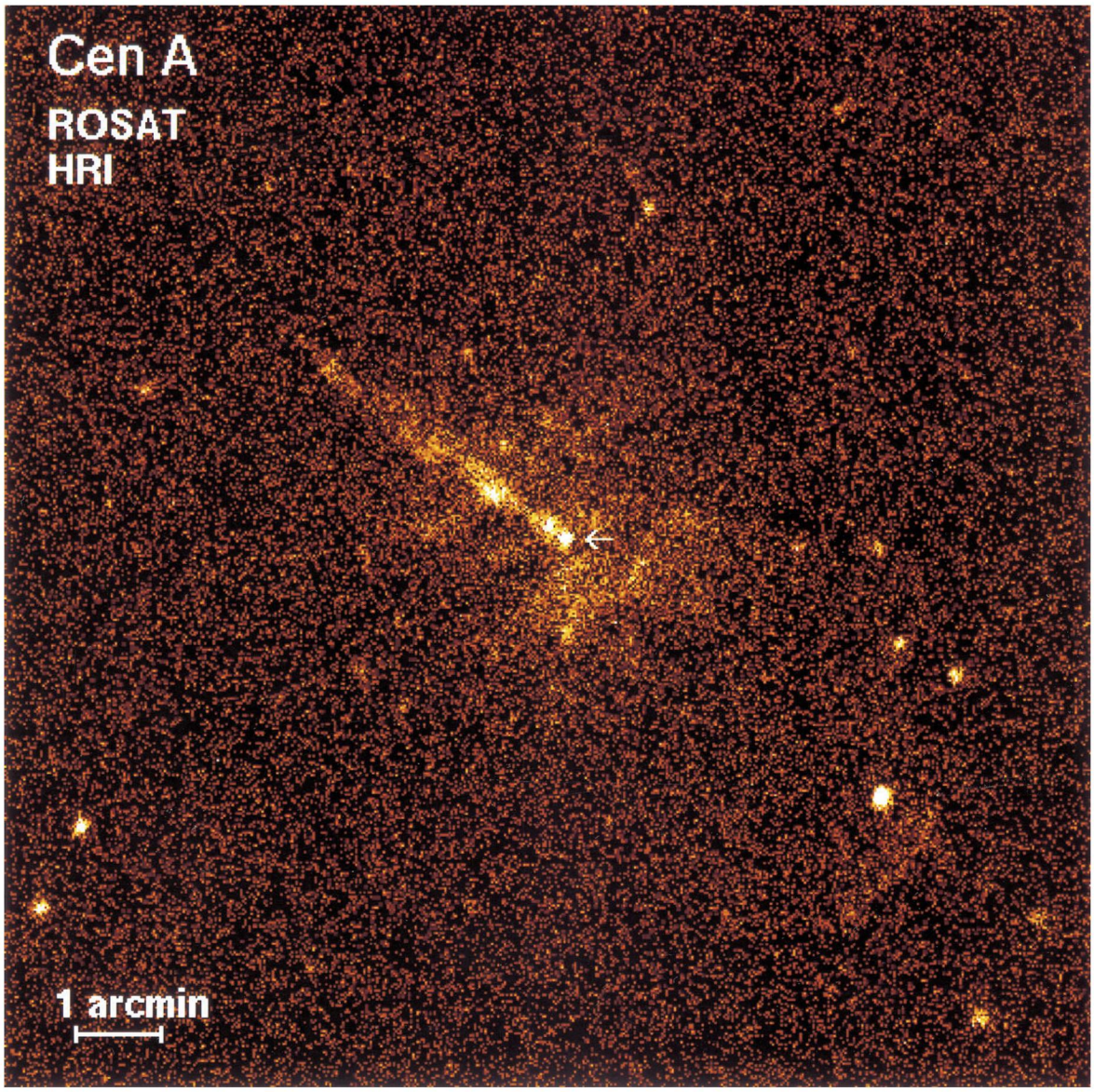

FIG. 1.—*ROSAT* HRI image of Cen A (sum of HRI observations in 1990 and 1994). The field size is 12.′8 × 12.′8; north is up, and east is to the left. The nucleus is marked with an arrow.

DÖBEREINER et al. (see 470, L15)

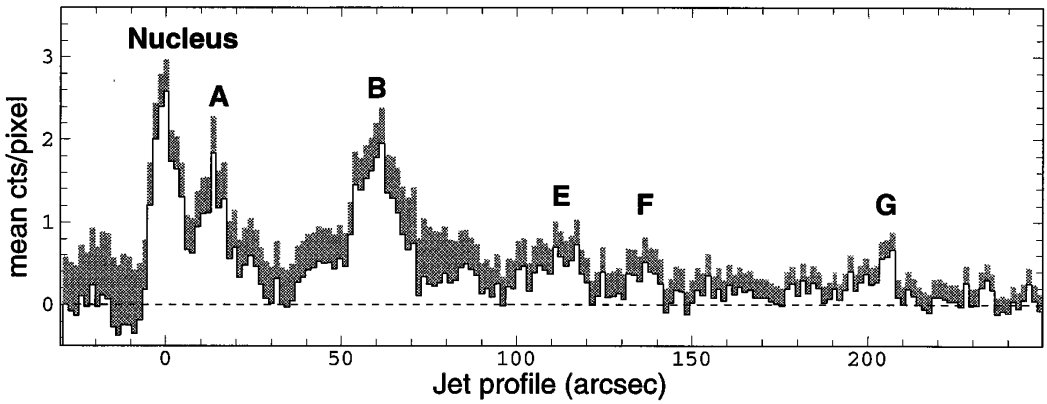

FIG. 4.—Background-subtracted profile of the X-ray jet (the shaded histogram represents the profile before background subtraction). The nucleus and the brightest knots are marked according to the nomenclature of Feigelson et al. (1981). The bin size along the jet is 1.″5.

12.′8 × 12.′8; north is up, and east is to the left. The image is not smoothed to show individual photons.

Figure 2 (Plate L3) shows an overlay of contours from a smoothed X-ray image on an optical image from the Digitized Palomar Sky Survey. The X-ray image was smoothed with an adaptive Gaussian filter algorithm, using a Gaussian σ of 17″ for the regions of lower surface brightness (about 95% of the image) and consecutively narrower Gaussian filters for higher surface brightness regions. The lowest three contours correspond to 3, 6, and 12 σ above background for extended emission.

Figure 3 (Plate L4) is an overlay of the X-ray contours on the 18 cm radio map of Clarke et al. (1992).

In the following we will describe the different X-ray features in comparison to their counterparts in other wavelengths.

3.1. *Nucleus and Jet*

Figure 4 shows the background-subtracted profile of the jet along the jet axis. The profile was integrated in a box 30″ wide, oriented along the jet (P.A. 55°), using the long observation in 1994 August. The background was obtained by extracting profiles in 30″ wide boxes to either side of the jet, averaging, smoothing, and scaling them to match the brightness of the underlying diffuse halo southwest of the nucleus. The shaded histogram in Figure 4 shows the profile before background subtraction.

The nucleus is the bright source at the southwestern end of the jet. The negative residuals after background subtraction southwest of the nucleus are due to the irregular distribution of the absorbing material, which shows up in the optical as an irregular dust lane. The profile of knot A may also be affected by this absorption. Judging from the absorption of the diffuse emission near the jet, we estimate the absorption to be of the order of 50% where the dust lane crosses the jet. The remaining uncertainty in the profile of knot A after background subtraction, due to the irregularity of the dust lane, is estimated to be on the order of 10% of the peak intensity.

The knot designation follows the nomenclature of Feigelson et al. (1981) and Clarke et al. (1992). In the *ROSAT* HRI data, knots C and D as identified by Feigelson et al. (1981) do not appear as individual knots. These knots also do not show up in the radio data, whereas all others are clearly discernible (Fig. 3). Knots C and D were excluded from further analysis. Further interknot X-ray emission can clearly be seen between knots F and G, whereas there is no significant emission outside knot G, where the radio jet blends into the inner northeastern radio lobe.

Figure 5 shows the transverse profiles of the nucleus and the knots. Superposed on each profile is a template profile obtained from the brightest point source in the field, shifted and scaled approximately to the knots' peak intensities. The template profile is consistent with the HRI point-spread function plus an additional artificial extent introduced by the attitude uncertainty of the *ROSAT* spacecraft (about 2″–3″ in this observation).

The nucleus of Cen A in X-rays is compatible with a point source. Knot A is marginally extended in both directions. Knot B is clearly extended along the direction of the jet. Knots E, F, and G are diffuse and extended, both along and perpendicular to jet. A Kolmogorov-Smirnov test, comparing the transversal profiles of the point source and the knots and taking into account possible errors in central position and background subtraction, gave extent probabilities of 4%, 55%, 66%, 96%, 94%, and 62% for the nucleus and knots A, B, E, F, and G respectively. Table 1 lists the locations of the nucleus and the knots. The locations correspond to the intensity maxima of the knots. Also listed are the position angles and distances with respect to the nucleus of Cen A.

The X-ray counts of the knots were derived by integrating the background-subtracted profiles shown in Figure 4. The luminosities were calculated assuming isotropic emission, a distance of 3.5 Mpc, a power-law spectrum with spectral (energy) index of $\alpha = 0.7$, and an absorbing neutral hydrogen column density $N_H = 10^{21}$ cm^{-2}. Table 1 gives the luminosities in the 0.1–2.4 keV spectral range for the nucleus and for the individual knots.

The luminosity of the nucleus in the *ROSAT* band (0.1–2.4 keV) increased significantly between the shorter observation in 1990 July [$(2.7 \pm 1.3) \times 10^{38}$ ergs s^{-1}, assuming Galactic absorption only] and the longer one in 1994 August [$(6.3 \pm 0.6) \times 10^{38}$ ergs s^{-1}]. This suggests that the bulk of the X-ray emission originates very close to the nucleus. The nucleus itself is assumed to be strongly absorbed ($N_H \approx 10^{23}$ cm^{-2}). With such a high absorption, the observable flux would be suppressed by a factor of 500 in the HRI energy range compared to the Galactic foreground absorption, raising the intrinsic nuclear luminosity to more than $L_X = (2–3) \times 10^{41}$ ergs s^{-1} (0.1–2.4 keV) in 1994. However, this value for N_H, which is frequently cited in the literature, originates from a spectral fit to an older, spatially unresolved *UHURU* observa-

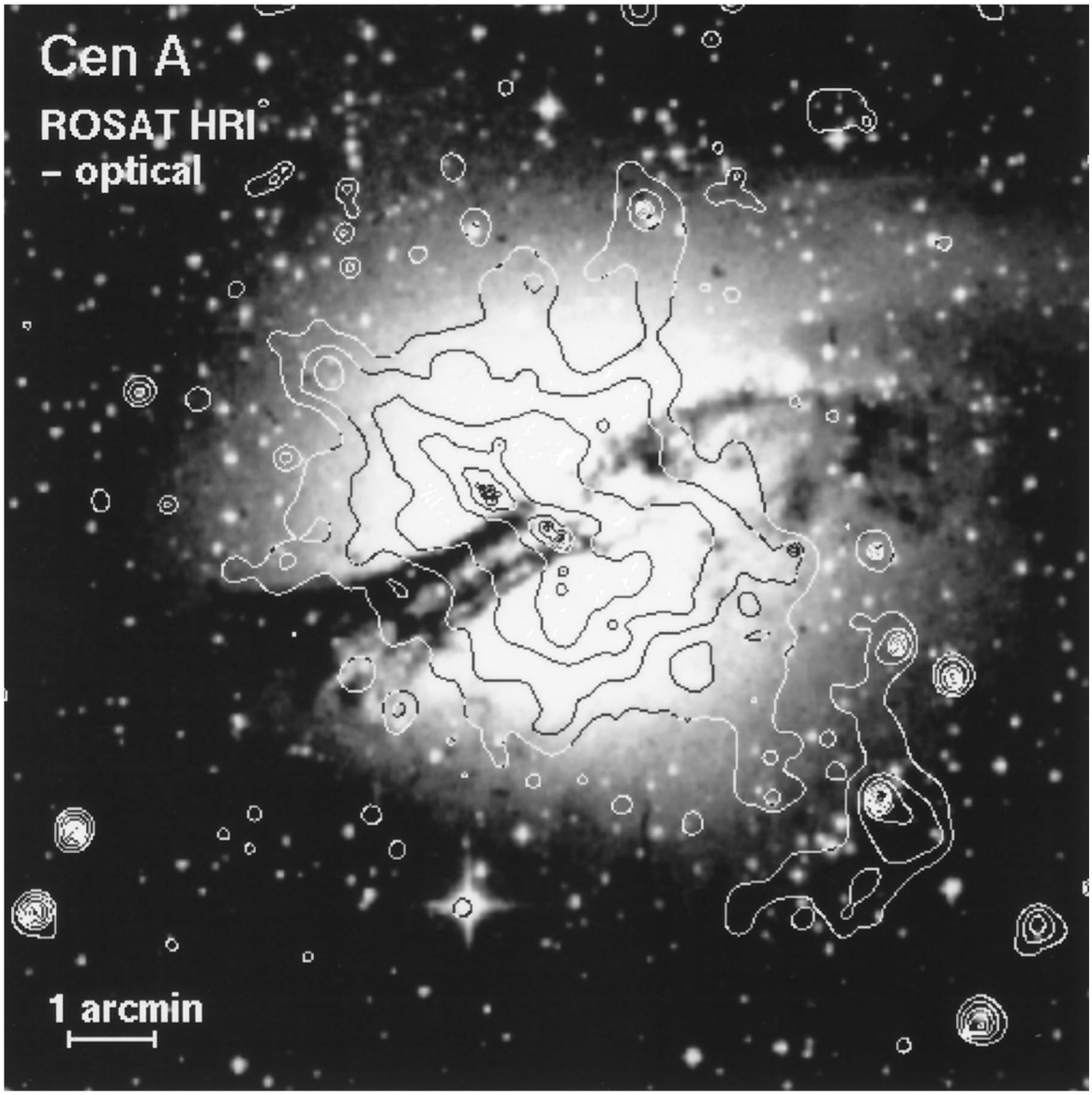

FIG. 2.—X-ray contour map (smoothed with an adaptive Gaussian filter) overlaid on an optical image of Cen A from the Palomar Digitized Sky Survey. The field size is 12.′8 × 12.′8; north is up, and east is to the left. The lowest three contour levels correspond to 3, 6, and 12 σ above background.

DÖBEREINER et al. (see 470, L16)

PLATE L4

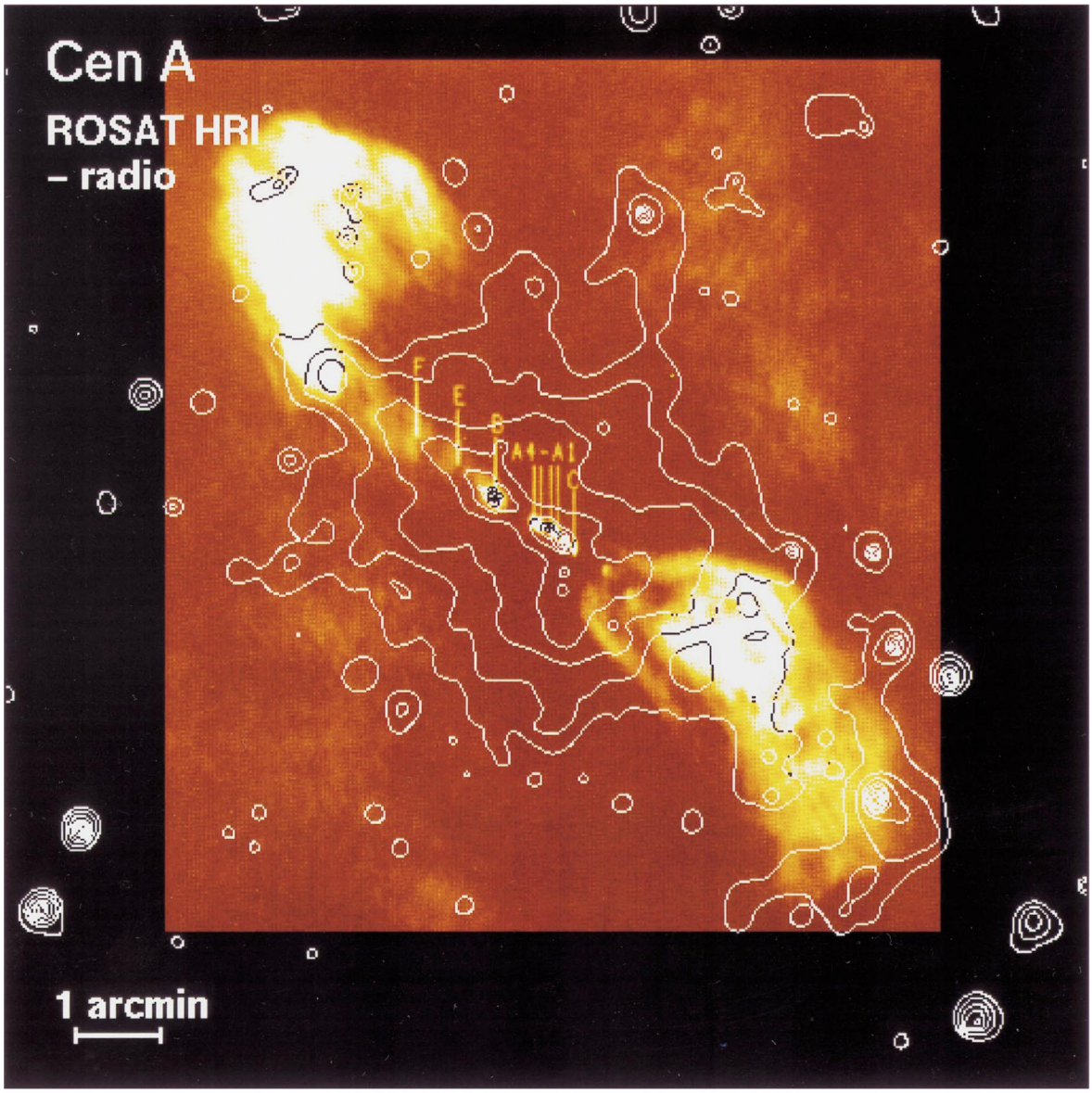

FIG. 3.—X-ray contour map overlaid on an 18 cm radio map (from Clarke, Burns, & Norman 1992). The field size is 12.′8 × 12.′8; north is up, and east is to the left.

DÖBEREINER et al. (see 470, L16)

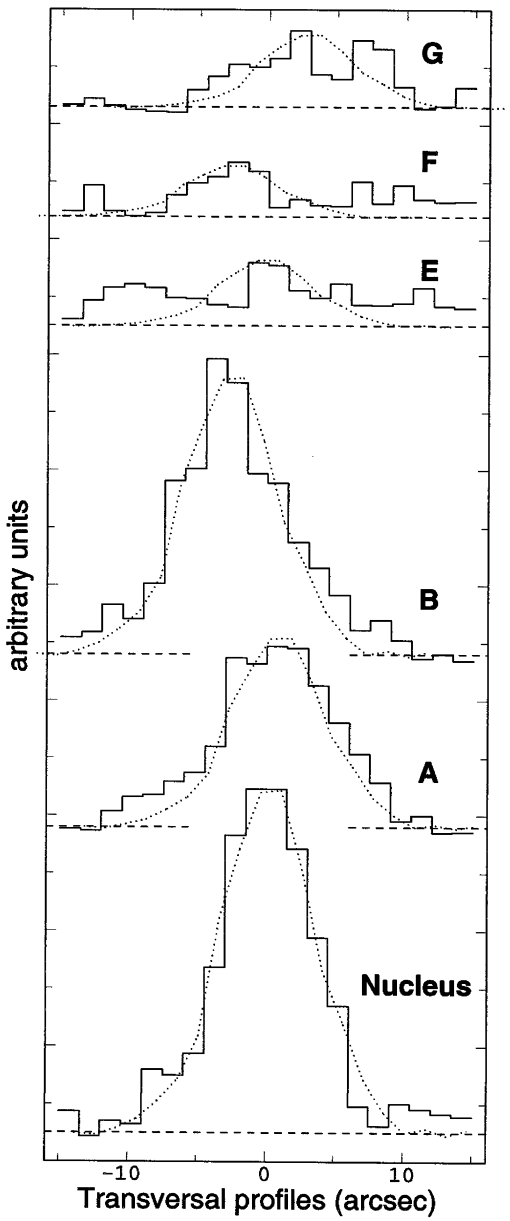

FIG. 5.—Background-subtracted transversal profiles of the nuclear source and the knots, offset along the *y*-axis for clarity. Dashed lines denote the zero levels; the dotted lines represent the profile of a comparison point source scaled to the peak intensity of each source.

tion of Cen A (Tucker et al. 1973) and may be substantially in error. *ROSAT* PSPC spectra of the nucleus are contaminated by emission both of the nearby knot A and of the diffuse halo. They also indicate a high intrinsic N_H but cannot constrain its exact value.

The luminosities of the knots within the X-ray jet of Cen A did not change between the 1990 and 1994 observations within the error margins, confirming the variability of the nuclear source.

The spectral resolution of the HRI is marginally sufficient for the detection of differences between the amplitude channel spectra of the background and those of the knots and the nucleus. Nucleus and knots generally show a harder spectrum than the diffuse (background) emission. But it is not sufficient to show significant differences among the spectra of individual knots. The PSPC with its better spectral resolution cannot resolve the individual knots in the X-ray jet. The necessary combination of sufficient spatial and spectral resolution will be provided by future X-ray missions like *AXAF* or *XMM*.

3.2. *Southwestern X-Ray Feature*

Opposite to the jet, about 5′.5 southwest of the nucleus, an extended diffuse feature is visible in Figure 1. Superposed on it is a bright unrelated X-ray point source that coincides with the location of a 14 mag foreground star. The brightest parts of the extended feature show up as an arclike structure just outside the southwestern inner radio lobe in the contour plot of Figure 3. The proximity to the outer edge of the radio lobe suggests that the feature consists of hot interstellar matter, probably from the gaseous halo of Cen A, which is compressed or shocked and heated by the expanding inner radio lobe. Similar interactions have been observed with *ROSAT* in Perseus A (Böhringer et al. 1993) and Cygnus A (Carilli, Perley, & Harris 1994).

The polarization map of the inner radio lobes (Fig. 5 of Clarke et al. 1992) shows significant polarization along and aligned with the outer edge of the southwestern radio lobe, whereas the northeastern radio lobe is less polarized and the polarization direction is not aligned along the outer edge. This supports the idea of interaction between the interstellar medium of Cen A and the southwestern radio lobe (see discussion in Wagner, Döbereiner, & Junkes 1995). A similar feature at the outer boundary of the northeastern lobe cannot be found.

After subtraction of the background and of the bright point source, the X-ray feature has 660 ± 100 counts in total in the long HRI observation. Assuming a distance of 3.5 Mpc, a Galactic absorption column $N_H = 10^{21}$ cm^{-2}, and a Raymond-Smith spectrum with temperature 0.5 keV and half-solar metallicity, this corresponds to a total luminosity of $(6.4 \pm 1.0) \times 10^{38}$ ergs s^{-1} (0.1–2.4 keV).

Imaging observations with the *EXOSAT* LE detector in the energy band 0.1–2 keV have also been interpreted to show a diffuse X-ray feature at the position of the southwestern radio lobe (Morini, Anselmo, & Molteni 1989). However, the reported *EXOSAT* feature has a structure different from the feature detected by us in approximately the same energy band. Furthermore, its luminosity was reported as 2×10^{39} ergs s^{-1}, higher by a factor of 3 compared to the *ROSAT* HRI detection. Since temporal variations seem unlikely, we conclude that the *EXOSAT* detection was at least in part due to confusion with the bright X-ray point source nearby.

3.3. *Associated Point Sources*

In the total HRI field of view we detect about 30 individual point sources with at least 5 σ, using a maximum likelihood technique. Some of the point sources in the field may be associated with foreground objects. However, the average density of sources in the field is much higher than the source densities observed in similar *ROSAT* observations away from the Galactic plane. Furthermore, the source distribution is centered on Cen A. We estimate that about 70%–80% of them are associated with Cen A. The luminosities of the detected sources are on the order of 10^{38} ergs s^{-1}. Identification of the sources is in progress.

TABLE 1

POSITIONS, COUNT RATES, AND LUMINOSITIES OF THE JET COMPONENTS

COMPONENT OR KNOT	P.A. (deg)	Distance (arcsec)	Integration Range[a] (arcsec)	Total Counts	0.1–2.4 keV Luminosity (10^{38} ergs s^{-1})
Nucleus[b]	...	0	−6.75–6.75	274 ± 27	6.3 ± 0.6
A	49	14	6.75–33.75	236 ± 36	5.4 ± 0.8
B[c]	58	60	33.75–93.75	505 ± 80	11.6 ± 1.8
E	56	111	93.75–122.25	140 ± 30	3.2 ± 0.7
F	56	136	122.25–141.75	69 ± 21	1.6 ± 0.5
Between F and G	...	...	141.75–188.25	76 ± 37	1.8 ± 0.9
G	54	204	188.25–210.75	83 ± 15	1.9 ± 0.3
Outside G	...	...	210.75–282.75	26 ± 29	0.6 ± 0.7

[a] Integration in box along P.A. 55°.
[b] 1994 August observation. Luminosities calculated under assumption of Galactic absorption only.
[c] Including locations of knots C and D as observed by *Einstein*.

3.4. *Diffuse Emission*

Figures 1 and 2 show a roughly circular halo of diffuse emission. It is evident from Figure 2 that the absorption seen in the X-ray data closely matches the visual absorption indicated by the dust lane. Feigelson et al. (1981) reported the existence of two ridges of diffuse emission parallel to the dust lane, explained by emission from unresolved point sources located in the dust and gas disk. Our data suggest that these ridges are merely the unabsorbed edges of the smooth diffuse halo where they adjoin the absorbed region.

The exact radial profile and total luminosity of the diffuse emission of Cen A have to await a detailed background model for this observation. At this stage it is not possible to differentiate between a hot gaseous halo and integrated emission of unresolved point sources. In particular, unresolved X-ray binaries associated with the gas and dust lane might contribute significantly to the observed diffuse emission.

However, we can give a rough estimate of $(9 \pm 3) \times 10^{39}$ ergs s^{-1} (0.1–2.4 keV, assuming 0.5 keV thermal emission and half-solar metallicity) for the total luminosity of the diffuse emission within a radius of 12′, corrected for the absorption by the dust lane. Assuming that all of the diffuse emission comes from a hot gaseous halo, Cen A is still underluminous in this respect compared to the mean (linear) L_X-L_B relation for early-type galaxies (Canizares, Fabbiano, & Trinchieri 1987).

If all the diffuse emission comes from unresolved discrete stellar sources (assuming $\alpha = 0.7$ power-law spectra with a different counts-to-flux ratio in comparison to thermal emission-line spectra), the total luminosity in the HRI energy band is calculated to 2×10^{40} ergs s^{-1}, which is twice (but compatible within the uncertainties) the luminosity expected for discrete sources within an early-type galaxy of $L_B = 10.5$ (Canizares et al. 1987).

4. SUMMARY

With the new X-ray data of Cen A, we can improve significantly on previous results and clearly distinguish different components of soft X-ray emission. We give luminosities and profiles for the nucleus and jet components (knots), and report the detection of a new diffuse X-ray feature, probably due to interaction of the southwestern inner radio lobe with the hot ISM of Cen A.

We wish to thank the *ROSAT* team for their outstanding technical and software support. The *ROSAT* project is supported by the Bundesministerium für Forschung und Technologie (BMFT/DARA) and the Max-Planck-Gesellschaft. The Digitized Sky Survey was produced at the Space Telescope Science Institute under US Government grant NAG W-2166. The optical image is based on photographic data obtained with the UK Schmidt Telescope.

REFERENCES

Böhringer, H., Voges, W., Fabian, A. C., Edge, A. C., & Neumann, D. M. 1993, MNRAS, 264, L25
Burns, J. O., Feigelson, E. D., & Schreier, E. J. 1983, ApJ, 273, 128
Canizares, C. R., Fabbiano, G., & Trinchieri, G. 1987, ApJ, 312, 503
Carilli, C. L., Perley, R. A., & Harris, D. E. 1994, MNRAS, 270, 173
Clarke, D. A., Burns, J. O., & Norman, M. L. 1992, ApJ, 395, 444
Feigelson, E. D., Schreier, E. J., Delvaille, J. P., Giacconi, R., Grindlay, J. E., & Lightman, A. P. 1981, ApJ, 251, 31
Hui, X., Ford, H. C., Ciardullo, R., & Jacoby, G. H. 1993, ApJ, 414, 463
Junkes, N., Haynes, R. F., Harnett, J. I., & Jauncey, D. L. 1993, A&A, 269, 29
Morini, M., Anselmo, F., & Molteni, D. 1989, ApJ, 347, 750
Thomson, R. C. 1992, MNRAS, 257, 689
Tingay, S. J. 1994, Australian J. Phys., 47, 619
Tucker, W., Kellogg, E., Gursky, H., Giacconi, R., & Tananbaum, H. 1973, ApJ, 180, 715
Wagner, S. J., Döbereiner, S., & Junkes, N. 1995, in Röntgenstrahlung from the Universe, ed. H. U. Zimmermann, J. Trümper, & H. Yorke (MPE Rep. 263; Garching: MPE), 521